



Ecosystem functioning is enveloped by hydrometeorological variability

Postprint version

Christoforos Pappas, Miguel D. Mahecha, David C. Frank, Flurin Babst
and Demetris Koutsoyiannis

Published in: **Nature Ecology & Evolution**

Reference: Pappas, C., Mahecha, M. D., Frank, D. C., Babst, F., & Koutsoyiannis, D. (2017). Ecosystem functioning is enveloped by hydrometeorological variability. *Nature Ecology & Evolution*, 1(9), 1263-1270. doi:10.1038/s41559-017-0277-5

Web link: <http://dx.doi.org/10.1038/s41559-017-0277-5>



This project has received funding from the European Union's Horizon 2020 research and innovation programme under grant agreement No 640176

Ecosystem functioning is enveloped by hydrometeorological variability

Christoforos Pappas^{1*}, Miguel D. Mahecha^{2,3}, David C. Frank^{4,5}, Flurin Babst^{4,6}
and Demetris Koutsoyiannis⁷

Terrestrial ecosystem processes, and the associated vegetation carbon dynamics, respond differently to hydrometeorological variability across timescales, and so does our scientific understanding of the underlying mechanisms. Long-term variability of the terrestrial carbon cycle is not yet well constrained and the resulting climate–biosphere feedbacks are highly uncertain. Here we present a comprehensive overview of hydrometeorological and ecosystem variability from hourly to decadal timescales integrating multiple in situ and remote-sensing datasets characterizing extra-tropical forest sites. We find that ecosystem variability at all sites is confined within a hydrometeorological envelope across sites and timescales. Furthermore, ecosystem variability demonstrates long-term persistence, highlighting ecological memory and slow ecosystem recovery rates after disturbances. However, simulation results with state-of-the-art process-based models do not reflect this long-term persistent behaviour in ecosystem functioning. Accordingly, we develop a cross-time-scale stochastic framework that captures hydrometeorological and ecosystem variability. Our analysis offers a perspective for terrestrial ecosystem modelling and paves the way for new model–data integration opportunities in Earth system sciences.

The atmosphere and biosphere are intrinsically coupled subsystems of the Earth¹. Hydrometeorological conditions shape ecosystem processes, which, in turn, affect the local, regional and global climate (for example, albedo feedbacks, modulations of land–atmosphere water and energy fluxes, seasonality in atmospheric CO₂). Hydrometeorological variability has been extensively studied² and short- and long-term variability in climate data have been widely assessed^{3,4}. With some notable exceptions primarily focusing on shorter timescales and/or individual sites^{5–9}, much less work has been undertaken to quantify the continuum of variability in ecosystem functioning across timescales. Key uncertainties remain in describing how variations in short-term physiological processes, such as photosynthesis¹⁰, influence subsequent processes such as carbon allocation¹¹ and remobilization¹², and then, ultimately, inter-annual to long-term ecosystem variability.

Here we present a comprehensive overview of the continuum of hydrometeorological and ecosystem variability, that is, the variability of ecosystem process related to vegetation carbon dynamics, across sites and timescales. We analyse data from 23 extra-tropical forest sites covering different climatic zones and vegetation characteristics, and we examine timescales spanning five orders of temporal magnitude, from hourly to decadal variability (Fig. 1).

‘Variability’ is intuitively quantified with the estimator of standard deviation (σ). The continuum of variability describes how σ changes with averaging timescale (k), denoted as $\sigma^{(k)}$, and is illustrated in the double-logarithmic space $\log(k)$ versus $\log(\sigma^{(k)})$, a graph known as a climacogram¹³. The advantages of this approach over other mathematically equivalent tools, such as power spectrum and variogram, are the very intuitive interpretation, the robust statistical estimation and the possibility to jointly analyse different datasets¹⁴. The continuum of variability represents the relative vari-

ability decay with timescale instead of using isolated values of individual variables or timescales. Therefore, several cross-correlated datasets can be represented together, after applying appropriate linear transformations, to extend the continuum of variability to longer timescales. Moreover, we derive a mathematically tractable, stochastic modelling framework that allows us to provide a quantitative interpretation and a parsimonious modelling of the observed cross-scale patterns of variability (see Methods).

Micrometeorological measurements of precipitation (P), air temperature (T), shortwave radiation (R) and vapour pressure deficit (D) are used to describe hydrometeorological variability at the analysed forest sites from hourly to annual timescales. The continuum of hydrometeorological variability is extended to the decadal timescale using reanalysis data for P , T , R and D , extracted for the examined locations (see Methods). Ecosystem variability is quantified using essential ecosystem variables, namely, long-term (≥ 10 yr) eddy covariance flux data of hourly net ecosystem exchange (NEE) of CO₂ between land surface and atmosphere, monthly remote sensing measurements of leaf area index (LAI) and fraction of absorbed photosynthetically active radiation (FPAR), annual tree-ring widths (TRW) and site-level above-ground biomass increment estimates (AGB), which are available for five of the analysed forests (Fig. 1b; see Methods).

We construct the relative ecosystem variability continuum by concatenating the timescales of NEE variability with those of LAI, FPAR, TRW and AGB data. We scrutinize their common relative variability decay patterns, even if the variables themselves reflect different aspects of ecosystem processes and dynamics. NEE data capture high-frequency variations of ecosystem carbon fluxes exchanged between atmosphere and the biosphere¹⁵ and describe ecosystem variability from hourly to inter-annual timescales^{5–8}.

¹Département de Géographie and Centre d'Études Nordiques, Université de Montréal, Montréal, QC H2V 2B8, Canada. ²Max Planck Institute for Biogeochemistry, 07745 Jena, Germany. ³German Centre for Integrative Biodiversity Research (iDiv) Halle-Jena-Leipzig, 04103 Leipzig, Germany. ⁴Swiss Federal Research Institute, WSL, 8903 Birmensdorf, Switzerland. ⁵Laboratory of Tree-Ring Research, University of Arizona, Tucson, Arizona 85721-0045, USA. ⁶W. Szafer Institute of Botany, Polish Academy of Sciences, 31-512 Krakow, Poland. ⁷Department of Water Resources and Environmental Engineering, School of Civil Engineering, National Technical University of Athens, 15780 Athens, Greece. *e-mail: christoforos.pappas@umontreal.ca

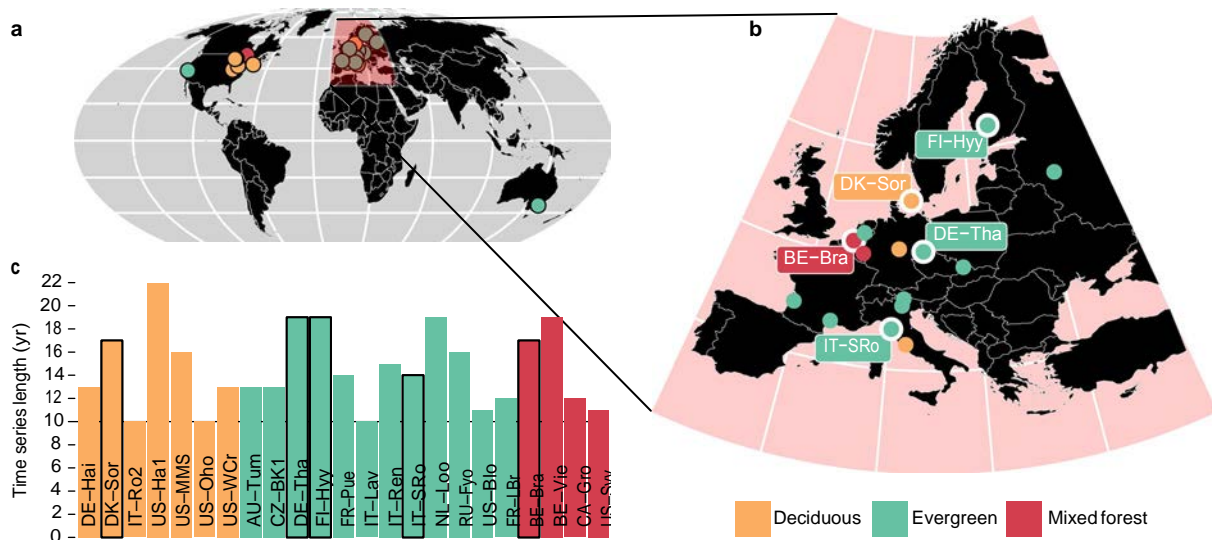


Fig. 1 | Spatial distribution of the analysed forest sites. **a**, The 23 sites with long-term (≥ 10 yr) micrometeorological and NEE measurements. **b**, European sites for which TRW and AGB data are also available (white circles). **c**, Length of the analysed time series of micrometeorological and eddy covariance measurements (the five European sites with additional measurements are highlighted in black). Different colours correspond to different forest types.

Currently, the longest NEE time series are approximately 20 yr (Fig. 1c), allowing characterization of the ecosystem variability continuum from hourly up to biennial timescales (see Methods). Remote sensing data of vegetation indices, such as LAI and FPAR, are tightly related to vegetation carbon dynamics (for example, light use efficiency models use FPAR to derive vegetation carbon fluxes¹⁶ and stocks¹⁷). Therefore, these vegetation indices can be used as proxies of ecosystem functioning extending the ecosystem variability continuum from intra-annual to triennial timescales with a 30-yr-long LAI and FPAR time series¹⁸. At these timescales, carbon fluxes and remote sensing vegetation indices should be tightly interconnected and can therefore be expected to show similar patterns of variability. At longer timescales, TRW and AGB data reveal annual tree growth and biomass dynamics and provide estimates of forest carbon dynamics that converge to observed NEE across several forests worldwide^{19–22}. The length of TRW and AGB time series at the five analysed forest sites ranges from 41 to 111 years²⁰ (Fig. 1b), therefore, the annual to decadal ecosystem variability at these sites can be sufficiently captured (see Methods).

results

We find that most hydrometeorological drivers display a similar pattern of variability from hourly to inter-annual timescales across all sites, except for P , which is also well-known for its high spatial variability^{3,4} (Fig. 2b–e). However, such convergence across sites is not reflected in the ecosystem variability (NEE, Fig. 2a, as well as for individual NEE components, Supplementary Fig. 3). Although the continuum of ecosystem variability follows a similar pattern across all the analysed sites (consistent drops in standard deviation at specific timescales), site-specific vegetation phenology dictates the magnitude of the standard deviation at intra-annual timescales. Seasonal ecosystem variability at deciduous forest sites is therefore larger compared to evergreen forest sites. This is a result of the pronounced phenological cycles of the former, whereas at forest sites with mixed vegetation phenology, seasonal ecosystem variability falls between the variability of evergreen and deciduous forest sites (Fig. 2a). Furthermore, NEE, R , T and D with pronounced periodical cycles at diurnal or annual scales show characteristic drops in their standard deviation at these very timescales, together with discontinuities (spikes) at half the period of the harmonic cycle

($\tau / 2$), as well as at timescales k equal to $m\tau / 2$, $m \in \mathbb{Z}$. This pattern is caused by the interplay of daily and annual harmonic cycles and can be described analytically (see Methods).

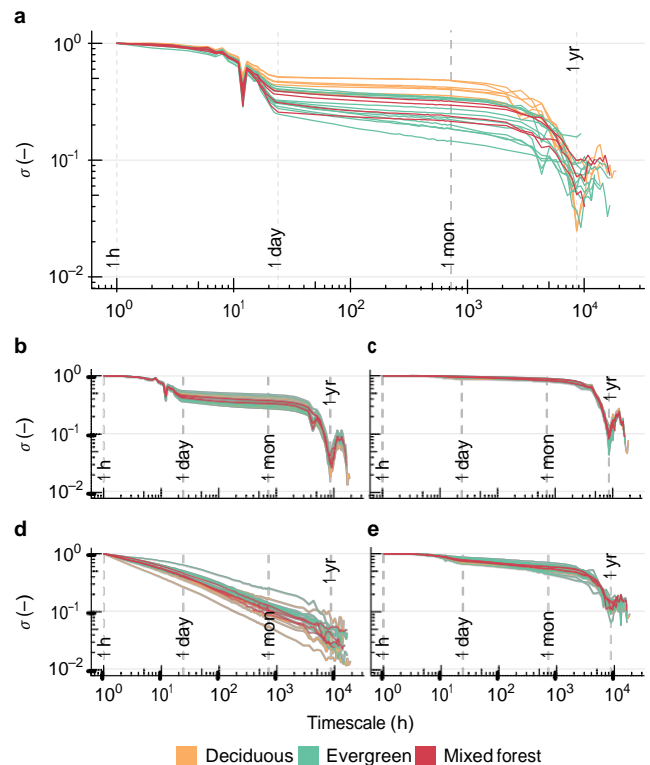


Fig. 2 | Ecosystem and hydrometeorological variability based on eddy covariance and micrometeorological data, respectively. **a–e**, Standard deviation (σ) as a function of the averaging timescale for NEE (**a**) as well as for the hydrometeorological drivers, namely R (**b**), T (**c**), P (**d**) and D (**e**), from hourly to inter-annual timescales for the 23 sites (Fig. 1). Data are standardized (zero mean and unit variance at the hourly timescale) so that patterns of variability can be compared across sites. Different colours correspond to different forest types.

By superimposing the continuum of variability of the analysed ecosystem variables, namely NEE, LAI, FPAR, TRW and AGB, we obtain a composite cross-scale ecosystem variability continuum from one hour to one decade (Fig. 3a). The composed variability continuum is consistent, as confirmed by the close match between the variability of individual ecosystem variables at the overlapping timescales (Fig. 3a; see Supplementary Fig. 10 for a quantitative assessment). More specifically, as illustrated in Fig. 3a for an example forest site, the standard deviation of NEE, as well as the standard deviations of LAI and FPAR from two independent remote sensing products, overlap at monthly to inter-annual timescales. Similarly, the standard deviation of TRW and AGB closely matches the standard deviation of NEE at the annual to biennial timescales, and the standard deviation of LAI and FPAR at the annual to triennial timescales (Fig. 3a). Therefore, despite the fact that different variables represent specific, yet tightly interwoven aspects of ecosystem func-

tioning, the overall ecosystem variability across timescales may now be approximated by the variability in NEE, LAI and TRW data for hourly-to-monthly, monthly-to-annual and annual-to-decadal timescales, respectively (Fig. 3a). Micrometeorological measurements, compiled together with reanalysis climate data, describe the continuum of variability of P , T , R and D from one hour to one decade (Fig. 3b). The use of several reanalysis datasets allows us to provide a better description of the hydrometeorological variability, accounting for uncertainties related to different products and gridding algorithms²³ (see Methods).

Overall, we find that ecosystem variability is confined within a hydrometeorological envelope that describes the range of variability of the available resources, that is, water and energy (Fig. 4). The hydrometeorological envelope emerges from the continua of variability of individual hydrometeorological variables (Fig. 3b). For an example site, a one-order-of-magnitude increase in the

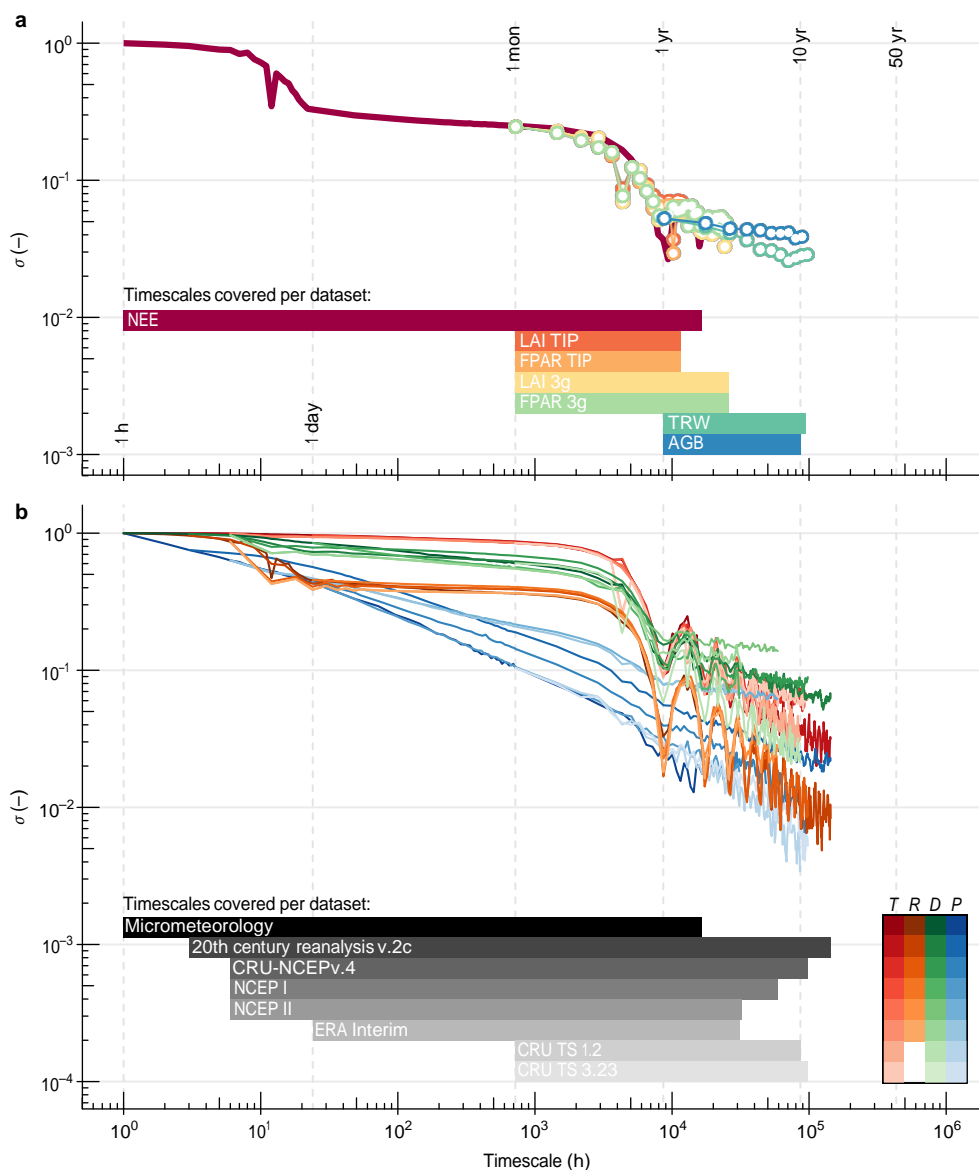


Fig. 3 | Composite ecosystem and hydrometeorological variability continua. **a**, Ecosystem variability (y axis) from hourly to decadal timescales of an example site (DE-Tha; Fig. 1b), as revealed by the superposition of several ecosystem variables (that is, NEE, LAI and FPAR from MODIS TIP and GIMMS 3g, TRW and AGB). **b**, The hydrometeorological envelope of this site, based on the variability continua of individual hydrometeorological variables (that is, P , D , R and T). Different colours correspond to different ecosystem and hydrometeorological variables. Horizontal bars highlight the timescales covered by each dataset.

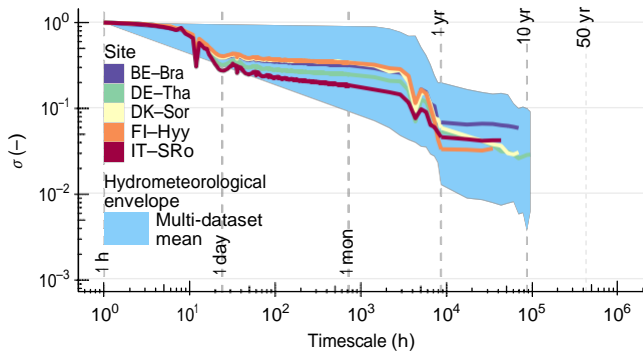


Fig. 4 | the hydrometeorological envelope of ecosystem variability continuum. Lines merge information at multiple timescales: eddy covariance flux measurements (NEE; 1 h–1 mon), remote sensing data (LAI 3g; 1 mon–1 yr), and tree-ring widths (TRW; 1 yr–10 yr) and represent the continuum of ecosystem variability at five forest ecosystems in Europe (coloured lines; Fig. 1b). The shaded blue area represents the hydrometeorological envelope of variability at these five sites and it is quantified by several state-of-the-art hydrometeorological datasets (Methods; coarser increments in x axis are used to enhance clarity).

timescale (for example, from one day to one month; x axes in Fig. 3) leads to a fivefold decrease in the standard deviation of precipitation (lower bound of the envelope) and to a mild decrease in the standard deviation of temperature by approximately 10% (upper bound of the envelope; y axis in Fig. 3b), whereas the standard deviation of ecosystem functioning shows a slight decrease by approximately 15% (y axis in Fig. 3a). Fig. 4 illustrates the hydrometeorological envelope of ecosystem variability continua at five European forest sites where TRW and AGB data are available (Fig. 1b). The slopes of the entire continuum of P , T , R and D variability, when compared to those of the ecosystem variability continua at the 23 analysed forest sites, provide a quantitative description of the hydrometeorological envelope in which ecosystem variability is confined (Supplementary Fig. 15). Steep slopes of P variability describe the lower limit of the hydrometeorological envelope and slight slopes of R and T variability the upper limit, whereas the slopes of ecosystem variability continua fall within the range of slopes of the hydrometeorological variables (Supplementary Fig. 15).

Furthermore, ecosystem variability demonstrates long-term persistence. Although absolute values of ecosystem variability differ across sites as a result of different climate, vegetation composition and stand characteristics, the temporal dependences exhibit the same behaviour across the entire range of analysed timescales (Fig. 4). The lower end of the continuum of ecosystem variability shows a slight slope, indicating long-term persistence in ecosystem functioning (Fig. 5a). Yet, simulation results with state-of-the-art Dynamic Global Vegetation Models (DGVMs, TRENDY multi-model ensemble²⁴; see Methods) do not reflect this pattern (Fig. 5b, Supplementary Fig. 12 and Supplementary Fig. 13d for TRENDY-derived ecosystem variability continuum is consistent with the composite of observations at intra-annual timescales, yet diverges substantially at inter-annual or longer timescales. At these scales, ecosystem variability simulated with the TRENDY multi-model ensemble has a much steeper decrease than what observations indicate (Fig. 5, Supplementary Fig. 13). Therefore, the simulated continua of both NEE (Fig. 5b) and net primary productivity (Supplementary Fig. 13d) variability approach the lower limit of the hydrometeorological envelope (that is, P variability), with the former exhibiting steeper variability decay than the latter, and contradict observational evidence of long-term persistence in

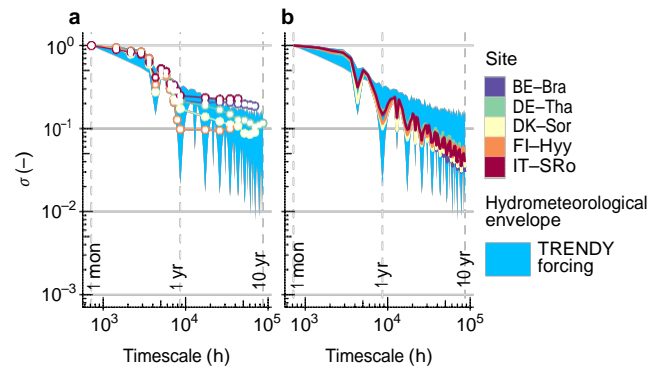


Fig. 5 | Empirical versus simulated continua of ecosystem variability. **a,b**, A comparison of observation-based (that is, composite of NEE, LAI 3g, and TRW data; **a**) and simulated (TRENDY multi-model mean simulated NEE; **b**) cross-scale ecosystem variability (y axes) across sites (coloured lines). The shaded area denotes the hydrometeorological envelope of the TRENDY climate forcing (CRU-NCEP v.4). For clarity, data are standardized so that they have zero mean and unit variance at the monthly timescale.

ecosystem functioning (that is, upper limit of the envelope, close to R and T variability).

To further investigate the properties and controls of ecosystem and hydrometeorological variability, we develop a stochastic modelling framework to simulate the observed patterns of variability across timescales. A combination of deterministic harmonics and stochastic processes (Fig. 6; see Methods) allows us to analytically describe the observed patterns (for example, the imprint of harmonic cycles on ecosystem variability across timescales or the magnitude of its low-frequency variability), and to further investigate the properties and controls of ecosystem and hydrometeorological variability. Diurnal and annual cycles correspond to variability continua of harmonic functions with periods $T_1 = 24$ h ($\sigma_{T_1}^{(k)}$) and $T_2 = 1$ yr ($\sigma_{T_2}^{(k)}$), respectively (Fig. 6a). The deterministic harmonics are then combined with three structurally different stochastic processes, namely, a purely random process (white noise; abrupt drop in standard deviation as timescale increases, corresponding to processes with no memory), a Markovian process (autoregressive model of order one, AR(1), reflecting processes with short-term persistence), and a Hurst–Kolmogorov (HK) process with long-term persistence (Fig. 6b). The continuum of variability of the latter ($\sigma_{HK}^{(k)}$) combined with that of the two harmonic functions, $\sigma_{T_1}^{(k)}$ and $\sigma_{T_2}^{(k)}$ (that is, $a\sigma_{T_1}^{(k)} + b\sigma_{T_2}^{(k)} + c\sigma_{HK}^{(k)}$, where a , b and c are weighting factors) are completely sufficient to describe the observed ecosystem and hydrometeorological variability from hourly to decadal timescales (Fig. 6c,d, see Methods). The close agreement between simulated and observed patterns of ecosystem variability brings quantitative evidence for the magnitude of long-term persistence in ecosystem functioning (Supplementary Fig. 15).

Discussion

As the timescale increases, hydrometeorological and ecosystem variability decreases. However, hydrometeorological conditions frame an envelope that constrains the continuum of ecosystem variability within its boundaries. We find that ecosystem variability exhibits a slight decrease as timescale increases, highlighting the impact of low-frequency variability in ecosystem functioning. Precipitation defines the lower limit and energy (that is, temperature and radiation) the upper limit of plausible variability regimes, with the resulting ecosystem variability being confined within these boundaries across sites and timescales. Low-frequency ecosystem variability has pronounced implications for our understanding of ecosystem stability and resilience²⁵, because it denotes

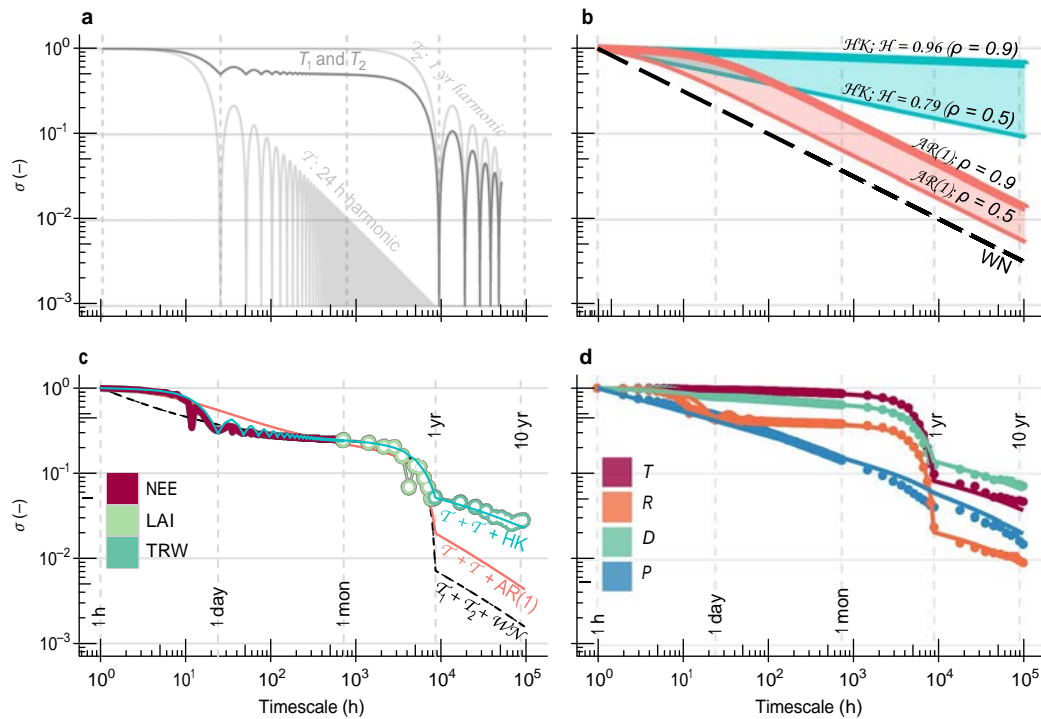


Fig. 6 | a parsimonious stochastic framework for modelling ecosystem and hydrometeorological variability across timescales. **a**, Theoretical values of σ versus averaging timescale for single (deterministic) harmonics with periods $T_1 = 24$ h, $T_2 = 1$ yr and a process with two harmonic cycles T_1 and T_2 . Theoretical values of σ versus averaging timescale for white noise (WN) and stochastic processes with short- (AR(1)), or long-term (Hurst–Kolmogorov) persistence for various values of Hurst coefficient (H) and lag-1 autocorrelation (ρ). **c**, Empirical ecosystem variability across timescales of an example site (DE–Tha, coloured points; Fig. 1b) based on eddy covariance flux measurements (NEE; 1 h–1 mon), remote sensing data (LAI 3g; 1 mon–1 yr), and tree-ring widths (TRW, 1 yr–10 yr; Fig. 3a), together with the fitted theoretical models (dashed and solid lines; $T_1 + T_2 + \text{WN}$, $T_1 + T_2 + \text{AR}(1)$, and $T_1 + T_2 + \text{HK}$). **d**, Empirical (coloured points) and fitted theoretical (solid lines) variability across timescales for each hydrometeorological variable at the DE–Tha site.

ecological memory^{26,27} and slow ecosystem recovery rates after disturbances^{25,28}. For instance, a steep decay of ecosystem variability with timescale (processes with no or a short memory) would indicate fast ecosystem recovery rates after disturbances (that is, enhanced resilience), but both theoretical²⁶ and observational evidence reported in the ecological literature rather suggest substantial memory effects in ecosystem functioning (for example, after drought stress²⁷). This pattern epitomizes the slow recovery rates of forest ecosystems and their susceptibility to tipping points²⁵. It is also expected that changes in the hydrometeorological drivers, for example in the frequency and severity of climate extremes¹, could alter the hydrometeorological envelope and affect the cross-scale continuum of ecosystem variability^{29,30}.

DGVMs offer a process-based representation of terrestrial ecosystem dynamics, integrating our current ecophysiological understanding. However, a bottom-up modelling of terrestrial ecosystem functioning is challenging, particularly when long-term predictions are envisioned³¹. While DGVMs capture intra-annual ecosystem variability adequately, ecosystem variability simulated with the TRENDY multi-model ensemble²⁴ does not reflect the pattern derived from the composed observational data at inter-annual to decadal timescales. We acknowledge that the composite of cross-scale ecosystem variability is approximated using various datasets of vegetation carbon dynamics while it ideally should be based on multi-decadal NEE measurements, which are, however, not currently available. Yet, over long timescales net exchange rates of ecosystems are expected to have a similarly persistent behaviour compared to the TRW variations. Hence, the observed discrepancy leads us to the hypothesis that processes influencing low-frequency variability in ecosystem functioning are either insufficiently con-

strained or not included in current DGVMs. For example, stand demographic processes and the resulting age-related variability in tree growth are rarely simulated in many DGVMs³², with some notable exceptions^{33,34}. However, apart from the five analysed forest sites where tree-ring data are available, low-frequency variability is also revealed with remote sensing data from the remaining 18 sites (Supplementary Fig. 15). This underlines that, apart from stand demography, other factors will contribute to persistence in ecosystem functioning. In particular, the interplay of plant ecophysiological processes relating carbon supply (photosynthesis; source activity) and carbon demand (tissue expansion; sink activity) is yet to be realistically described in DGVMs^{35–37} and is known to substantially affect the low-frequency variability in the terrestrial carbon cycle. A mechanistic understanding of the interplay between environmental drivers (for example, water³⁸, CO_2 ³⁹ and nutrients⁴⁰) and ecophysiological response (resource allocation and remobilization^{11,12}, plant acclimation and plasticity^{41,42}) is still to be consolidated, leading to well-documented structural and parameterization issues in DGVMs^{37,43} that could eventually explain the steep decay in the TRENDY-simulated ecosystem variability continuum. Moreover, the mismatch between the spatial scale of DGVM input (for example, climate forcing and initial conditions) and the resolution of the DGVM simulation grid hampers the parameterization of fine-scale processes and results in aggregation biases in the simulated terrestrial carbon dynamics^{44,45}. Finally, several processes with well-documented impact on terrestrial carbon fluxes and stocks are also not yet adequately represented in state-of-the-art DGVMs (for example, leaf mesophyll conductance⁴⁶, carbon turnover rates⁴⁷ and soil microbial activity⁴⁸), and may affect cross-scale ecosystem variability.

We derive an analytical model, combining deterministic harmonics and stochastic processes, that represents major mechanisms and uncertainties and mimics the observed pattern of hydrometeorological and ecosystem variability. Additional natural (for example, wildfires or insect outbreaks) or anthropogenic (for example, forest management) mechanisms, that may affect the variability of certain ecosystems, can also be incorporated in the aforementioned framework by including theoretical representations of their cross-scale variability according to the observed patterns. This stochastic modelling framework offers a parsimonious and mathematically tractable approach for understanding and modelling ecosystem variability across sites and timescales, overcoming the aforementioned limitations of DGVMs. Furthermore, this framework reflects well the observed ecological memory, an inherent property of ecosystem functioning, therefore enhancing the ecological realism in numerical simulations.

The presented analysis offers a perspective for understanding and modelling of the variability of the terrestrial carbon cycle and paves the way for new model–data integration opportunities in Earth system sciences. DGVMs are incorporated in Earth System Models to simulate the terrestrial ecosystem dynamics and climate–biosphere feedbacks⁴⁹. Therefore, poorer fidelity of low-frequency variability in the former will be propagated to simulation results with the latter, leading to potential biases in the resulting climate projections⁵⁰. While model–data comparisons in terms of relative, rather than absolute, variability are widespread, so far the focus has been on individual timescales (for example, monthly or annual anomalies of observed compared to simulated variables). However, analysing and modelling the interplay between hydrometeorological drivers and ecosystem response requires developing a joint framework across multiple sites and timescales. Therefore, we advocate to formalize and implement a cross-scale model–data integration approach. The presented continuum of ecosystem variability offers an independent emerging observational constraint for Earth System Models⁴⁹ and the projected terrestrial carbon source–sink dynamics²⁴. Moreover, the derived hydrometeorological envelope defines the boundaries of plausible climate–carbon cycle sensitivities allowing for a predic-

and climate–biosphere feedbacks^{1,31}.

Methods

Datasets. Hydrometeorological drivers. Time series of P , T , R and D are used to quantify hydrometeorological variability (Supplementary Table 2). Micrometeorological data, obtained from FLUXNET2015 (December 2015 release; <http://fluxnet.fluxdata.org/data/fluxnet2015-dataset/fullset-data-product/>), are compiled together with time series of the following reanalysis gridded products: ERA Interim⁵¹, NCEP I (ref. ⁵²) and II (ref. ⁵³), 20th century reanalysis v2c^{54–56}, CRU TS 1.2 (ref. ⁵⁷), CRU TS 3.23 (ref. ⁵⁸) and CRU–NCEP v4. The latter is a combination of CRU TS 3.21 and NCEP I, and is used for climate forcing of TRENDY simulations²⁴. Grid cells that correspond to the locations of the eddy covariance forest sites are selected (Supplementary Information).

Ecosystem response. Ecosystem variability is quantified based on multivariate proxies of ecosystem functioning (Supplementary Table 1), consisting of: (i) hourly NEE data (Supplementary Table 3); (ii) monthly LAI and FPAR time series from grid cells corresponding to the location of the eddy covariance forest sites, provided by the Moderate Resolution Imaging Spectroradiometer Two-stream Inversion Package⁵⁹ (MODIS TIP; time period: 2001–2014, Supplementary Fig. 5) and the third generation of Global Inventory Modelling and Mapping Studies¹⁸ (GIMMS 3g; time period: 1981–2011, Supplementary Fig. 6); and (iii) TRW (Supplementary Fig. 7) and AGB²⁰ (Supplementary Fig. 8) available at five European sites (Fig. 1b). The pattern of variability of the partitioned hourly NEE data to gross primary productivity and ecosystem respiration is also examined (Supplementary Information). Moreover, the observed pattern of ecosystem variability is compared with simulated monthly NEE from TRENDY v.1 multi-model ensemble²⁴ (Fig. 5), as well as additional simulated variables (Supplementary Information).

Statistical analysis. Empirical climacograms. The continuum of hydrometeorological and ecosystem variability is quantified by examining

how the (sample) standard deviation ($\sigma^{(k)}$) of various hydrometeorological and ecosystem variables changes across averaging timescales (k). The values of k range from the original temporal resolution of each dataset (Δ) to $L/10$ where L is the total length of the time series¹³, therefore allowing at least 10 values for the estimation of $\sigma^{(k)}$ at $k = L/10$. In order to compare hydrometeorological and ecosystem variability across sites and variables, data are standardized, that is, zero mean and unit variance at the original timescale (for example, $\Delta = 1\text{h}$ for micrometeorological and NEE measurements, Fig. 2a; $\Delta = 1\text{ month (mon)}$ for LAI and FPAR, Supplementary Figs. 5, 6; and $\Delta = 1\text{yr}$ for TRW and AGB, Supplementary Fig. 9).

Composite climacograms. Linear transformations are applied to construct the combined continuum of ecosystem and hydrometeorological variability. Cross-correlated variables that reflect ecosystem functioning at different timescales can be combined in a single climacogram after applying appropriate linear transformations. This allows us to compare how the standard deviation of different processes varies and co-varies across ecosystems and timescales. For example, if the process of interest is ecosystem functioning ($y(t)$; where t denotes time) then NEE, LAI, FPAR, TRW and AGB can be seen as proxies of $y(t)$. These proxies are intrinsically related, and, as an approximation, we can assume that they are linearly connected. In other words, $y(t) = ax(t) + b$, where $x(t)$ can be any of the proxy variables NEE, LAI, FPAR, TRW or AGB. Therefore, it follows that $\sigma_y^{(k)} = a\sigma_x^{(k)}$. The close match of the variability of individual ecosystem variables at the overlapping timescales supports this approximation (Fig. 3a and Supplementary Fig. 10). Moreover, theoretical and observational evidence demonstrate the applicability of light use efficiency models to linearly relate LAI and FPAR with carbon uptake, therefore capturing the variability of vegetation carbon fluxes¹⁶ and stocks¹⁷.

More specifically, LAI and FPAR data are transformed so that $J_{\text{LAI,FPAR}}^{(k=1\text{mon})} = J_{\text{NEE}}^{(k=1\text{mon})}$ and TRW and AGB data are transformed so that $\sigma_{\text{TRW,AGB}}^{(k=1\text{yr})} = \sigma_{\text{LAI}}^{(k=1\text{yr})}$. Reanalysis hydrometeorological data are transformed so that the standard deviation of each hydrometeorological variable at the original timescale (Δ) matches the standard deviation of the same variable from the micrometeorological measurements at this timescale, for example, for the case of precipitation $\sigma_{\text{reanalysis},p}^{(k=i)} = \sigma_{\text{micromet},p}^{(k=i)}$ (Fig. 3b). The increments in the x axis of the hydrometeorological envelope depicted in Fig. 4 are coarser than Fig. 3b for the sake of clarity of Fig. 4, therefore the drops in standard deviation due to the diurnal and annual harmonic cycles are not visible (compare with Fig. 3b).

Theoretical climacograms. Once the underlying process is known, its continuum of variability can be derived analytically¹³. Fig. 6a depicts the theoretical variability across timescales for deterministic harmonic processes with different periods, τ , while Fig. 6b illustrates the variability across timescales for three structurally

harmonic process is given by:

$$\sigma^{(k)} = \frac{\sigma}{k} \left| \sin \frac{k}{2} \right| \text{ for } k = \left(m + \frac{1}{2} \right) \tau \text{ where } m \in \mathbb{Z} \quad (1)$$

For $k = \left(m + \frac{1}{2} \right) \tau$ there is a discontinuity in the continuum of variability (for example, spikes for $k = 12\text{h}$ for the case of diurnal cycle, or $k = 6\text{ mon}$ for the annual cycle in Fig. 2; Supplementary Information). A purely random process (white noise; WN) and two widely used stochastic processes in geophysics, namely, (i) a Markovian process characterized by short-term persistence and (ii) a Hurst–Kolmogorov process with long-term persistence, are also examined. The standard deviation of white noise decays with k as follows:

$$J_{\text{WN}}^{(k)} = \frac{J}{\sqrt{k}} \quad (2)$$

where σ denotes the standard deviation at the original timescale. For Markovian process, described by an autoregressive model of order one, AR(1) with lag-1 autocorrelation (ρ), $\sigma^{(k)}$ is given by:

$$\sigma_{\text{AR}(1)}^{(k)} = \frac{\sigma}{\sqrt{k}} \sqrt{\frac{(1-\rho^2) - 2\rho(1-\rho^k) + \rho^{2k}}{(1-\rho)^2}} \quad (3)$$

whereas for the Hurst–Kolmogorov (HK) process, $\sigma^{(k)}$ is equal to:

$$J_{\text{HK}}^{(k)} = k^{H-1} J \quad (4)$$

where H is the Hurst coefficient ($H = 0.5(\log_2(\rho + 1) + 1)$). The continuum of variability of AR(1) and Hurst–Kolmogorov process present distinct patterns. The former is characterized by a fast decay that is equal to white noise for large timescales, whereas the latter shows slight slopes as a result of long-term persistence (Fig. 3b).

Model fitting. Theoretical climacograms are fitted to empirical estimates of standard deviation ($\sigma^{(k)}$) accounting for biases in $\sigma^{(k)}$ due to sample size (L). Bias in $\sigma^{(k)}$ can be estimated a priori analytically¹⁵ and is equal to:

$$E[\sigma^{(k)}] = \frac{y^{(k)} - y^{(L)}}{1 - k/L}$$

A model, $J_y^{(k)}$, is assumed based on a linear combination of $(J_{T_1}^{(k)}, J_{T_2}^{(k)}, J_{WN}^{(k)}, J_{AR(1)}^{(k)}, J_{HK}^{(k)})$, that is,

$$J_y^{(k)} = \begin{cases} aJ_{T_1}^{(k)} + bJ_{T_2}^{(k)} + cJ_{WN}^{(k)} \\ aJ_{T_1}^{(k)} + bJ_{T_2}^{(k)} + cJ_{AR(1)}^{(k)} \\ aJ_{T_1}^{(k)} + bJ_{T_2}^{(k)} + cJ_{HK}^{(k)} \end{cases}$$

Weighting factors a , b and c , as well as lag-1 autocorrelation (ρ), for the case of AR(1), or Hurst coefficient (H), for the case of the Hurst–Kolmogorov process, are fitting parameters adjusted so that the sum of squared errors is minimized numerically (Supplementary Information). For the model fitting of the ecosystem variability continuum (Fig. 6c), theoretical models are fitted to the composite empirical ecosystem continuum as described by NEE (1 h–1 mon), LAI 3g (1 mon–1 yr), and TRW (1 yr–10 yr), where available. Model fitting for each hydrometeorological variable (Fig. 6d) is conducted by fitting theoretical models to the mean empirical continuum of variability estimated as the mean of the micrometeorological, CRU–NCEP v.4, and 20th century reanalysis v.2c datasets (Supplementary Information). These three datasets are selected because of the large overlap in the analysed timescales (Fig. 3b).

Code availability. The analysis was conducted in R version 3.3.2 and the scripts of the analysis are available from the corresponding author upon reasonable request.

Data availability. The micrometeorological, eddy covariance and remote sensing data that support the findings of this study are available from public repositories (see Supplementary Information). Tree-ring widths and site-level above-ground biomass increment estimates used in this study are available upon reasonable request to D.C.F. and F.B., respectively.

Received: 19 September 2016; Accepted: 23 June 2017;

Published online: 21 August 2017

references

1. IPCC *Climate Change 2013: The Physical Science Basis* (eds Stocker, T. F. et al.) (Cambridge Univ. Press, 2013).
2. Mitchell, J. M. Jr An overview of climate variability and its causal mechanisms. *Quat. Res.* **6**, 481–493 (1976).
3. Franke, J., Frank, D., Raible, C. C., Esper, J. & Brönnimann, S. Spectral biases in tree-ring climate proxies. *Nat. Clim. Change* **3**, 360–364 (2013).
4. Markonis, Y. & Koutsoyiannis, D. Scale-dependence of persistence in precipitation records. *Nat. Clim. Change* **6**, 399–401 (2016).
5. Baldocchi, D., Falge, E. & Wilson, K. A spectral analysis of biosphere–atmosphere trace gas flux and meteorological variables across hour to multi-year time scales. *Agric. For. Meteorol.* **107**, 1–27 (2001).
6. Katul, G. et al. Multiscale analysis of vegetation surface fluxes: from seconds to years. *Adv. Water Resour.* **24**, 1119–1132 (2001).
7. Mahecha, M. D. et al. Characterizing ecosystem–atmosphere interactions from short to interannual time scales. *Biogeosciences* **4**, 743–758 (2007).
8. Stoy, P. C. et al. Biosphere–atmosphere exchange of CO₂ in relation to climate: a cross-biome analysis across multiple time scales. *Biogeosciences* **6**, 2297–2312 (2009).
9. Mueller, K. L., Yadav, V., Curtis, P. S., Vogel, C. & Michalak, A. M. Attributing the variability of eddy-covariance CO₂ flux measurements across temporal scales using geostatistical regression for a mixed northern hardwood forest. *Global Biogeochem. Cycles* **24**, GB3023 (2010).
10. Farquhar, G. D., von Caemmerer, S. & Berry, J. A. A biochemical model of photosynthetic CO₂ assimilation in leaves of C3 species. *Planta* **149**, 78–90 (1980).
11. Franklin, O. et al. Modeling carbon allocation in trees: a search for principles. *Tree Physiol.* **32**, 648–666 (2012).
12. Hartmann, H. & Trumbore, S. Understanding the roles of nonstructural carbohydrates in forest trees—from what we can measure to what we want to know. *New Phytol.* **211**, 386–403 (2016).
13. Koutsoyiannis, D. Generic and parsimonious stochastic modelling for hydrology and beyond. *Hydrol. Sci. J.* **61**, 225–244 (2016).
14. Dimitriadis, P. & Koutsoyiannis, D. Climacogram versus autocovariance and power spectrum in stochastic modelling for Markovian and Hurst–Kolmogorov processes. *Stoch. Environ. Res. Risk Assess.* **29**, 1649–1669 (2015).
15. Baldocchi, D. et al. FLUXNET: a new tool to study the temporal and spatial variability of ecosystem-scale carbon dioxide, water vapor, and energy flux densities. *Bull. Am. Meteorol. Soc.* **82**, 2415–2434 (2001).
16. Hilker, T., Coops, N. C., Wulder, M. A., Black, T. A. & Guy, R. D. The use of remote sensing in light use efficiency based models of gross primary production: a review of current status and future requirements. *Sci. Total Environ.* **404**, 411–423 (2008).
17. Myneni, R. B. et al. A large carbon sink in the woody biomass of Northern forests. *Proc. Natl Acad. Sci. USA* **98**, 14784–14789 (2001).
18. Zhu, Z. et al. Global data sets of vegetation leaf area index (LAI)3g and fraction of photosynthetically active radiation (FPAR)3g derived from global inventory modeling and mapping studies (GIMMS) normalized difference vegetation index (NDVI3g) for the period 1981 to 2011. *Remote Sens.* **5**, 927–948 (2013).
19. Rocha, A. V., Goulden, M. L., Dunn, A. L. & Wofsy, S. C. On linking interannual tree ring variability with observations of whole-forest CO₂ flux. *Glob. Change Biol.* **12**, 1378–1389 (2006).
20. Babst, F. et al. Above-ground woody carbon sequestration measured from tree rings is coherent with net ecosystem productivity at five eddy-covariance sites. *New Phytol.* **201**, 1289–1303 (2014).
21. Campioli, M. et al. Evaluating the convergence between eddy-covariance and biometric methods for assessing carbon budgets of forests. *Nat. Commun.* **7**, 13717 (2016).
22. Delpierre, N., Berveiller, D., Granda, E. & Dufrene, E. Wood phenology, not carbon input, controls the interannual variability of wood growth in a temperate oak forest. *New Phytol.* **210**, 459–470 (2016).
23. Cavanaugh, N. R. & Shen, S. S. P. The effects of gridding algorithms on the statistical moments and their trends of daily surface air temperature. *J. Clim.* **28**, 9188–9205 (2015).
24. Sitch, S. et al. Recent trends and drivers of regional sources and sinks of carbon dioxide. *Biogeosciences* **12**, 653–679 (2015).
25. Scheffer, M., Carpenter, S. R., Dakos, V. & Van Nes, E. H. Generic indicators of ecological resilience: inferring the chance of a critical transition. *Annu. Rev. Ecol. Syst.* **46**, 145–167 (2015).
26. Ogle, K. et al. Quantifying ecological memory in plant and ecosystem processes. *Ecol. Lett.* **18**, 221–235 (2015).
27. Anderegg, W. R. L. et al. Pervasive drought legacies in forest ecosystems and their implications for carbon cycle models. *Science* **349**, 528–532 (2015).
28. Frank, D. et al. Effects of climate extremes on the terrestrial carbon cycle: concepts, processes and potential future impacts. *Glob. Change Biol.* **21**, 2861–2880 (2015).
29. Reyer, C. P. O. et al. A plant’s perspective of extremes: terrestrial plant responses to changing climatic variability. *Glob. Change Biol.* **19**, 75–89 (2013).
30. Reichstein, M. et al. Climate extremes and the carbon cycle. *Nature* **500**, 287–295 (2013).
31. Luo, Y., Keenan, T. F. & Smith, M. J. Predictability of the terrestrial carbon cycle. *Glob. Change Biol.* **21**, 1737–1751 (2015).
32. Fisher, R. et al. Assessing uncertainties in a second-generation dynamic vegetation model caused by ecological scale limitations. *New Phytol.* **187**, 666–681 (2010).
33. Medvigy, D., Wofsy, S. C., Munger, J. W., Hollinger, D. Y. & Moorcroft, P. R. Mechanistic scaling of ecosystem function and dynamics in space and time: Ecosystem Demography model version 2. *J. Geophys. Res.* **114**, G01002 (2009).
34. Scheiter, S., Langan, L. & Higgins, S. I. Next-generation dynamic global vegetation models: learning from community ecology. *New Phytol.* **198**, 957–969 (2013).
35. Faticchi, S., Leuzinger, S. & Körner, C. Moving beyond photosynthesis: from carbon source to sink-driven vegetation modeling. *New Phytol.* **201**, 1086–1095 (2014).
36. Körner, C. Paradigm shift in plant growth control. *Curr. Opin. Plant Biol.* **25**, 107–114 (2015).
37. Pappas, C., Faticchi, S., Leuzinger, S., Wolf, A. & Burlando, P. Sensitivity analysis of a process-based ecosystem model: pinpointing parameterization and structural issues. *J. Geophys. Res. Biogeosci.* **118**, 505–528 (2013).
38. Faticchi, S., Pappas, C. & Ivanov, V. Y. Modeling plant–water interactions: an ecohydrological overview from the cell to the global scale. *Wiley Interdiscip. Rev. Water* **3**, 327–368 (2016).
39. Pugh, T. A. M., Müller, C., Arneith, A., Haverd, V. & Smith, B. Key knowledge and data gaps in modelling the influence of CO₂ concentration on the terrestrial carbon sink. *J. Plant Physiol.* **203**, 3–15 (2016).
40. Fernández-Martínez, M. et al. Nutrient availability as the key regulator of global forest carbon balance. *Nat. Clim. Change* **4**, 471–476 (2014).
41. Aubin, I. et al. Traits to stay, traits to move: a review of functional traits to assess sensitivity and adaptive capacity of temperate and boreal trees to climate change. *Environ. Rev.* **24**, 164–186 (2016).
42. Lombardozi, D. L., Bonan, G. B., Smith, N. G., Dukes, J. S. & Fisher, R. A. Temperature acclimation of photosynthesis and respiration: a key uncertainty

- in the carbon cycle-climate feedback. *Geophys. Res. Lett.* **42**, 8624–8631 (2015).
43. Medlyn, B. E., Duursma, Ra & Zeppel, M. J. B. Forest productivity under climate change: a checklist for evaluating model studies. *Wiley Interdiscip. Rev. Clim. Change* **2**, 332–355 (2011).
 44. Potter, K. A., Arthur Woods, H. & Pincebourde, S. Microclimatic challenges in global change biology. *Glob. Change Biol.* **19**, 2932–2939 (2013).
 45. Pappas, C., Fatichi, S., Rimkus, S., Burlando, P. & Huber, M. The role of local-scale heterogeneities in terrestrial ecosystem modeling. *J. Geophys. Res. Biogeosci.* **120**, 341–360 (2015).
 46. Sun, Y. et al. Impact of mesophyll diffusion on estimated global land CO₂ fertilization. *Proc. Natl Acad. Sci. USA* **111**, 15774–15779 (2014).
 47. Friend, A. D. et al. Carbon residence time dominates uncertainty in terrestrial vegetation responses to future climate and atmospheric CO₂. *Proc. Natl Acad. Sci. USA* **111**, 3280–3285 (2014).
 48. Sulman, B. N., Phillips, R. P., Oishi, A. C., Shevliakova, E. & Pacala, S. W. Microbe-driven turnover offsets mineral-mediated storage of soil carbon under elevated CO₂. *Nat. Clim. Change* **4**, 1099–1102 (2014).
 49. Friedlingstein, P. & Prentice, I. C. Carbon–climate feedbacks: a review of model and observation based estimates. *Curr. Opin. Environ. Sustain.* **2**, 251–257 (2010).
 50. Ault, T. R., Cole, J. E. & St. George, S. The amplitude of decadal to multidecadal variability in precipitation simulated by state-of-the-art climate models. *Geophys. Res. Lett.* **39**, L21705 (2012).
 51. Dee, D. P. et al. The ERA-Interim reanalysis: configuration and performance of the data assimilation system. *Q. J. R. Meteorol. Soc.* **137**, 553–597 (2011).
 52. Kalnay, E. et al. The NCEP/NCAR 40-year reanalysis project. *Bull. Am. Meteorol. Soc.* **77**, 437–471 (1996).
 53. Kanamitsu, M. et al. NCEP-DOE AMIP-II reanalysis (R-2). *Bull. Am. Meteorol. Soc.* **83**, 1631–1643 (2002).
 54. Whitaker, J. S., Compo, G. P., Wei, X. & Hamill, T. M. Reanalysis without radiosondes using ensemble data assimilation. *Mon. Weather Rev.* **132**, 1190–1200 (2004).
 55. Compo, G. P., Whitaker, J. S. & Sardeshmukh, P. D. Feasibility of a 100-year reanalysis using only surface pressure data. *Bull. Am. Meteorol. Soc.* **87**, 175–190 (2006).
 56. Compo, G. P. et al. The twentieth century reanalysis project. *Q. J. R. Meteorol. Soc.* **137**, 1–28 (2011).
 57. Mitchell, T. D., Carter, T. R., Jones, P. D. & Hulme, M. A *Comprehensive Set of High-Resolution Grids of Monthly Climate for Europe and the Globe: the Observed Record (1901–2000) and 16 Scenarios (2001–2100)* Working paper no. 55 (Tyndall Centre for Climate Change Research, 2004).
 58. Harris, I., Jones, P. D., Osborn, T. J. & Lister, D. H. Updated high-resolution grids of monthly climatic observations-the CRU TS3.10 dataset. *Int. J. Climatol.* **34**, 623–642 (2014).
 59. Pinty, B. et al. Exploiting the MODIS albedos with the Two-Stream Inversion Package (JRC-TIP): 1. Effective leaf area index, vegetation, and soil properties. *J. Geophys. Res.* **116**, D09105 (2011).

acknowledgements

This work used eddy covariance data acquired and shared by the FLUXNET community, including these networks: AmeriFlux, AfriFlux, AsiaFlux, CarboAfrica, CarboEuropeIP, CarboItaly, CarboMont, ChinaFlux, Fluxnet-Canada, GreenGrass, ICOS, KoFlux, LBA, NECC, OzFlux-TERN, TCOS-Siberia and USCCC. The FLUXNET eddy covariance data processing and harmonization was carried out by the ICOS Ecosystem Thematic Center, AmeriFlux Management Project and Fluxdata project of FLUXNET, with the support of CDIAC, and the OzFlux, ChinaFlux and AsiaFlux offices. We thank the participants of the TRENDY project, namely, P. Levy (Hyland), S. Sitch and C. Huntingford (JULES/TRIFFID), B. Poulter (LPJ), A. Ahlström (LPJ-GUESS), S. Levis (NCAR-CLM4), N. Viovy, S. Zaehle (OCN), M. Lomas (SDGVM) and N. Zeng (VEGAS), who made their simulations results (TRENDY v.1, experiment S2) freely available. C.P. acknowledges the support of the Stavros Niarchos Foundation and the ETH Zurich Foundation (grant P2EZP2_162293) through a Swiss National Science Foundation (SNSF) Early Postdoc. Mobility fellowship. M.D.M., F.B. and D.C.F. acknowledge funding from the European Union via the Horizon 2020 project 'BACI' (grant 640176). F.B. acknowledges funding from the Swiss National Science Foundation (grant P300P2_154543).

author contributions

C.P. designed the study, conducted the analysis and wrote the manuscript with input from M.D.M. and D.K. D.C.F. provided the tree-ring width data and F.B. the above-ground biomass increment data. All authors contributed to editing the manuscript.

Competing interests

The authors declare no competing financial interests.

additional information

Supplementary information is available for this paper at doi:10.1038/s41559-017-0277-5.

Reprints and permissions information is available at www.nature.com/reprints.

Correspondence and requests for materials should be addressed to C.P.

Publisher's note: Springer Nature remains neutral with regard to jurisdictional claims in published maps and institutional affiliations.